UDC 551.511.3:551.513.2:551.509.334:551.465.7

Response of a Tropical Atmosphere and Ocean Model to Seasonally Variable Forcing[1,2]

ARTHUR C. PIKE[3]—*Rosenstiel School of Marine and Atmospheric Science, University of Miami, Coral Gables, Fla.*

ABSTRACT—The atmospheric part of a pre-existing, interacting atmosphere and ocean model has been simplified considerably to provide a 3-yr prediction of intertropical convergence zone (ITCZ) behavior under the influence of seasonally variable solar heating of the sea. As before in shorter term experiments, a cold equatorial surface appears and a single ITCZ develops north or south of the Equator over the surface temperature maximum in the warmer hemisphere. The ITCZ migrates quickly between hemispheres, lagging only slightly behind the seasonal reversal of the hemispheric surface temperature asymmetry. Such behavior is qualitatively in accord with that of the updraft branch of the mean tropical Hadley circulation in the real atmosphere. The lag of maximum subequatorial sea-surface temperature behind the overhead sun of late summer is computed to be 9 weeks, a reasonable value.

1. INTRODUCTION

A previous article by Pike (1971) has described the results of a two-fluid, primitive-equation experiment in which a simple, two-layer model of the upper tropical ocean was combined with a relatively complex, 10-level model of a zonally symmetric tropical atmosphere. The main objective was prediction of a north–south profile of sea-surface temperature and determination of the influence of surface temperature on the atmospheric intertropical convergence zone (ITCZ). Consideration of computational economy restricted the numerical integration to only 88 days of model time. For such a limited period (compared with 1 yr), the clear-sky solar insolation at the surface was assumed to be constant in time; it was prescribed as constant in latitude as well because of the model's limited north–south extent.

In the above experiment, the surface temperature profile, initially flat in the lower latitudes, developed a cold Equator as a result of upwelling and vertical mixing of colder water from below. A single ITCZ established itself over the Equator, then migrated poleward as the Equator cooled; the convergence zone remained single, showing great stability despite the eventual double surface-temperature maximum. The production of such a marked hemispheric asymmetry despite symmetric initial conditions and thermal forcing was ascribed to the action of very small numerical perturbations in the pressure computations or the inherent nature of the model ITCZ to prefer a single mode. This preference was also shown to be characteristic of the ITCZ in the real atmosphere.

It seemed desirable to integrate a similar two-fluid model over a period of several years so that we could investigate the degree of stability of the single off-equatorial ITCZ under the influence of seasonally variable solar heating of the sea. However, nearly 30 hr of Control Data Corporation[4] (CDC) 6600 computer time would have been required for a 1-yr prediction with the combined atmosphere and ocean model as it originally was constituted. Simplification was indicated for purposes of economy, but the oceanic part was really as basic as could safely be attempted in temperature prediction involving dynamic factors. Only the atmospheric part was suitable for reduction in complexity. The less complicated atmosphere model used in this experiment is discussed in section 2. It has only four atmospheric levels and handles frictional and convective processes in a much simpler way than was previously done. This model requires only about 1.5 hr on the CDC 6600 for a 1-yr prediction.

The oceanic part of the present model is almost identical to that used in the previous computations, and only an abbreviated reference is made to it in section 2. The results of some 3-yr experiments with this model are presented in section 3. Because overheating was evident in these experiments, other, shorter ones were made to demonstrate the control of surface temperature by adjusting such critical parameters as the surface drag coefficient and the vertical atmospheric diffusivity; these matters are also covered in section 3. A necessary comparison of these purely theoretical, computational findings with actual observations in the atmosphere and ocean by both conventional and satellite techniques appears in section 4.

2. DESCRIPTION OF THE SIMPLE, TWO-FLUID MODEL

The atmospheric part of the model is of a primitive-equation type and is constructed in a meridional cross-

[1] Contribution 1510 from the Rosenstiel School of Marine and Atmospheric Science, University of Miami, Coral Gables, Fla.

[2] This paper is a revision of part of the author's doctoral dissertation at the University of Miami.

[3] Now affiliated with the National Hurricane Center, NOAA, Coral Gables, Fla.

[4] Mention of a commercial product does not constitute an endorsement.

section with Cartesian coordinates perpendicular to a beta plane. Its domain extends between latitudes 30°S and 30°N and from sea level to the tropical tropopause just above 16 km. The horizontal spacing of the finite-difference grid is 2° of latitude, except next to the lateral boundaries where it is 4°. Vertical grid levels are at 0 and 10 m and at 1.057, 5.870, and 16.535 km. Space differencing is upstream for the advective terms but is centered for all other terms such as the mass divergence and pressure gradient; forward time differencing is used with a step, Δt, of 30 min, the largest possible with reliable computational stability.

Four predictive equations are used; they are the familiar momentum equations for the two horizontal velocity components, the first law of thermodynamics for potential temperature, and an equation of continuity for moisture. Vertical motion is computed from meridional motion using a steady-state approximation of the equation of mass continuity; the pressure field is obtained by assuming hydrostatic equilibrium. Explicitly, we have:

$$\frac{\partial u}{\partial t}=-u\frac{\partial u}{\partial x}-w\frac{\partial u}{\partial z}+fv-\frac{1}{\rho}\frac{\partial p}{\partial x}-\frac{1}{\rho}\frac{\partial F_u}{\partial z}+K_H\frac{\partial^2 u}{\partial x^2}, \quad (1)$$

$$\frac{\partial v}{\partial t}=-u\frac{\partial v}{\partial x}-w\frac{\partial u}{\partial z}-fu-\frac{1}{\rho}\frac{\partial F_v}{\partial z}+K_H\frac{\partial^2 v}{\partial x^2}, \quad (2)$$

$$\frac{\partial \theta}{\partial t}=-u\frac{\partial \theta}{\partial x}-w\frac{\partial \theta}{\partial z}+Q_L+Q_C+Q_R-\frac{1}{\rho}\frac{\partial F_\theta}{\partial z}+K_H\frac{\partial^2 \theta}{\partial x^2}, \quad (3)$$

$$\frac{\partial q}{\partial t}=-u\frac{\partial q}{\partial x}-w\frac{\partial q}{\partial z}+S_q-\frac{1}{\rho}\frac{\partial F_q}{\partial z}+K_H\frac{\partial^2 q}{\partial x^2}, \quad (4)$$

$$\frac{\partial}{\partial x}(\rho u)+\frac{\partial}{\partial z}(\rho w)=0, \quad (5)$$

and

$$\frac{\partial}{\partial z}\left(\frac{p}{p_0}\right)^\kappa=-\frac{g}{c_p\theta}. \quad (6)$$

Here, x represents a *northward*-directed coordinate and z, the vertical coordinate, u and v are respectively the *northward* and *westward* wind velocity components, and w is the vertical velocity component. The Coriolis parameter, f, is zero on the Equator, varying linearly with x according to a constant beta parameter of 2.19×10^{-13} $cm^{-1}\cdot s^{-1}$. The latent heat of condensation for water is denoted by L and g is the acceleration of gravity. Density, ρ, is computed from initial data by

$$\rho=\frac{p_0{}^\kappa p^{1-\kappa}}{R\theta} \quad (7)$$

where p_0 is the standard reference pressure of 1000 mb, p is variable pressure, θ stands for potential temperature, R is the specific gas constant for dry air, and $\kappa \equiv R/c_p$ where c_p is the specific heat of dry air. Density is held constant in time. Note that the effect of moisture on air density has been neglected. This simplification may be justified a posteriori by noting that all the ITCZs predicted by our model found stable locations over relatively warm surface waters where a maximum evaporative moisture source was available. Logically then, inclusion of this effect would have reduced the air density in the heart of the model ITCZ and probably increased its intensity somewhat but would not have changed its qualitative behavior.

F_u, F_v, F_θ, and F_q are respectively the vertical turbulent fluxes of specific momentum, sensible heat plus potential energy in terms of potential temperature, and moisture in terms of mixing ratio, q. We shall consider them to be positive upward. At the surface these fluxes are computed by the bulk transfer formula

$$F_s=(\rho C_D U)_{10}(s_0-s_{10}) \quad (8)$$

where s may be either u, v, θ, or q. C_D is the surface drag coefficient and U is the total horizontal wind speed. The subscripts 0 and 10 indicate values taken at the 0- and 10-m levels, respectively. In the interior of the model, an austausch formula is used to compute these fluxes; that is,

$$F_s=-\rho K_z\frac{\partial s}{\partial z} \quad (9)$$

where K_z is the constant vertical diffusivity. At the topmost model level, vertical fluxes are not computed, and their vertical gradient terms in the predictive equations are neglected.

Q_C represents the condensation heat source associated with atmospheric convection. We have modeled this very important process in a manner similar to that of Yamasaki (1968), assuming that convective latent heat release is directly proportional to the mean upward moisture flux, $\overline{F}_q \equiv \rho(w+|w|)q/2$. Convective heating in our model may occur only at the 1.057- and 5.870-km levels, denoted respectively by the subscripts b and a; Q_C is always zero elsewhere. Specifically,

$$Q_{Cb}=\frac{L}{c_p(\rho\Delta z)_b}\left(\frac{p_0}{p_b}\right)^\kappa \overline{F}_{qb}l$$

and (10)

$$Q_{Ca}=\frac{L}{c_p(\rho\Delta z)_a}\left(\frac{p_0}{p_a}\right)^\kappa [\overline{F}_{qb}(1-l)+\overline{F}_{qa}].$$

The mass per unit area between the level in question and that next level above is given by $\rho\Delta z$. The fraction of the upward moisture flux through the lower level, subscript b, assumed to condense between levels b and a is symbolized by l.

The latent heat release from large-scale condensation in the presence of supersaturation is given by Q_L where

$$Q_L=\frac{L}{c_p}\left(\frac{p_0}{p}\right)^\kappa \frac{[(q-q_s)+|q-q_s|]}{2\Delta t}. \quad (11)$$

Here, q_s is the saturation specific humidity and Δt is the computational time step. In conjunction with the first term of the moisture sink equation [eq (13)], this heating term provides for all moisture above the saturation amount to be condensed and rained out.

In any atmospheric model designed for integrations over many weeks of physical time, a radiational heat

467-299 O - 72 - 2

sink, Q_R, is necessary. It may be expressed as

$$Q_R=\left(\frac{p_0}{p}\right)^{\kappa}\left(\frac{\partial T}{\partial t}\right)_R \tag{12}$$

where $(\partial T/\partial t)$ is the local rate of change of temperature from all radiational effects. This rate of change may either be specified, say as a function of height only from the data of Smagorinsky et al. (1965), or computed. See section 3 for an example of such a computation.

An atmospheric moisture sink, S_q, accompanying the condensation process is included in the moisture continuity equation. It is expressed by

$$S_q=\frac{(q_s-q)-|q-q_s|}{2\Delta t}+w\frac{\partial q}{\partial z}\,s\,(Q_c\overline{F}_q) \tag{13}$$

where $s(x)=0$ for $x\leq 0$ and $s(x)=1$ for $x>0$. The first term represents the falling out of moisture associated with large-scale condensation heating, Q_L, and the second term indicates that all moisture advected upward in the presence of convectional heating, Q_C, is removed from the atmosphere. Note that liquid-water storage by clouds is neglected in this model.

Specification of horizontal turbulent mixing by the simplest method possible, using a constant horizontal diffusivity, K_H, completes the model's basic set of equations.

Determination of the vertical motion field requires vertical integration of eq (5) from the surface, where $w=0$ is assumed, to H, the top of the model. Level H is about at the tropical tropopause; consequently, the vertical motion is set to zero there too. This state is realized by requiring the total meridional mass transport, $\int_0^H \rho u dz$, to vanish everywhere; the final meridional velocity component, u, is obtained from the computed value, u_c, by the correction equation

$$u(z)=u_c(z)-\frac{\int_0^H \rho u_c dz}{\int_0^H \rho dz}. \tag{14}$$

The pressure field is obtained by downward integration of eq (6) from the model top to the surface. The pressure at the top, p_H, a function of latitude and time, is computed by noting that the height-averaged pressure,

$$\overline{p}\equiv\frac{1}{H}\int_0^H p dz,$$

may be integrated by parts to yield

$$p_H=\overline{p}-\frac{1}{H}\int_{p_H}^{p_s} z dp$$

where p_s is the surface pressure. Substitution of eq (6), the hydrostatic equation, into this expression yields

$$p_H=\overline{p}-\frac{gp_0^{\kappa}}{RH}\int_0^H \frac{p^{1-\kappa}z}{\theta}\,dz. \tag{15}$$

Once $\overline{p}$ is known, p_H may be found by trial and error, using eq (15) to obtain a hydrostatically consistent $p(z)$ profile from $z=0$ to $z=H$. The prerequisite calculation of the $\overline{p}(x)$ field is based on eq (1), the meridional momentum equation, rewritten in the form

$$\frac{\partial p}{\partial x}=-\frac{\partial \rho u}{\partial t}+\rho G \tag{16}$$

where G is defined by substitution of eq (16) into eq (1) assuming negligible local density change. Averaging eq (16) with respect to height, one obtains

$$\frac{\partial \overline{p}}{\partial x}=-\frac{1}{H}\frac{\partial}{\partial t}\int_0^H \rho u dz+\overline{\rho G};$$

the first right-hand-side term is seen to vanish because of the condition of zero total meridional mass transport. To have boundary conditions for $\overline{p}$ at latitude 30° in *both* hemispheres, we differentiated this expression with respect to x to yield

$$\frac{\partial^2 \overline{p}}{\partial x^2}=\frac{\partial}{\partial x}\,\overline{(\rho G)}. \tag{17}$$

Note that eq (17) may be obtained in a more general way from eq (16) by x-differentiation, substitution of the mass continuity eq (5), height-averaging, and the assumption that the vertical mass flux, ρw, is constant in time at both $z=0$ and $z=H$. This second-order equation is solved by a Gauss elimination method described in Richtmyer and Morton (1967, sec. 8.5). This method introduces the very small, hemispherically asymmetric, numerical perturbations mentioned in section 1. Numerical experiments have verified the occurrence of these perturbations at the sixth significant figure when the International Business Machines (IBM) 360/65 computer is used.

The boundary conditions of this model are relatively simple. On the lateral boundaries at latitudes 30°S and 30°N, u, v, θ, and q are specified as functions of height and time; the boundary pressure profile is computed at each time step by assuming a fixed surface pressure and then integrating upward hydrostatically to the top of the model. Vertical motion is set to zero at these latitudes. At the surface, all momentum components are assumed to vanish, the potential temperature corresponds to the temperature computed by the ocean model described below, and the specific humidity is set to its saturation value. On the top boundary, all the predictive equations [eq (1)–(4)] are applied, but there is assumed to be no vertical motion or vertical advection, no vertical flux gradients, no convective heating, and no corresponding moisture sink at that level.

The oceanic part of the model is the same as that described in Pike (1971, sec. 3) with the exception of the computation of the surface momentum and heat fluxes, in particular that of the incoming solar radiation. Equation (8) is used to obtain the surface wind stress components τ_{0x} and τ_{0y} for the ocean model; that is,

$$\tau_0(x, y)=(\rho C_D U)_{10}(u, v)_{10}. \tag{18a}$$

Likewise, the surface friction velocity, U_*, with respect to

water density is obtained from

$$U_*=\left[\frac{(\rho C_D)_{10}}{\rho_s}\right]^{1/2}U_{10}. \tag{18b}$$

The net downward heat flux at the sea surface, S, is obtained by the expression

$$S=\frac{R\downarrow-\epsilon\sigma T_s^4-c_p\left(\frac{p_s}{p_0}\right)^{\kappa}F_{\theta s}-LF_{qs}}{\rho_s c} \tag{19}$$

where ρ_s is the density of water, c is its specific heat, T_s is the sea-surface temperature, σ is the Stefan-Boltzmann constant, and $F_{\theta s}$ and F_{qs} are respectively the surface values of F_θ and F_q as computed by the atmosphere model. The incoming short-wave solar radiation, $R\downarrow$, and the net long-wave emissivity, ϵ, are obtained as in Pike (1971), eq (7) and (8); however, the average daily clear-sky short-wave radiation flux, R_0, and the cloudiness, n, are computed as described below.

Seasonal variation of the surface solar heating is accomplished by letting R_0 vary with time and latitude according to the approximate expression

$$R_0=R_{00}\left(\frac{\pi}{2}\sin\phi\sin\delta+\cos\phi\cos\delta\right) \tag{20}$$

where $R_{00}=33.271\times10^{-3}$ J·cm^{-2}·s^{-1} is the equatorial equinoctial value of R_0, obtained from Budyko (1958). The latitude is denoted by ϕ, and the solar declination, δ, is computed by

$$\delta=23.45^\circ\sin 2\pi\left(\frac{t+t_p}{t_y}\right) \tag{21}$$

where t_p is a thermal lag time and t_y is the length of 1 yr. Using data from the atmosphere model, we have computed n according to the formula

$$q_r\equiv\frac{1}{H}\int_0^H\left(\frac{q}{q_s}\right)dz \tag{22}$$

where

$$\begin{Bmatrix} n=0.0 \text{ if } q_r\leq 0.2 \\ n=(q_r-0.2)/0.6 \text{ if } 0.2<q_r<0.8 \\ n=1.0 \text{ if } q_r\geq 0.8 \end{Bmatrix}.$$

This type of dependence of cloudiness on vertically averaged relative humidity has been taken from Smagorinsky (1960) with the critical values of 20 and 80 percent estimated from his figure 1.

3. RESULTS OF THE LONG-TERM INTEGRATIONS

Ideally, a combined atmosphere and ocean model should be computed over a period of physical time long enough for it to reach statistical equilibrium in the ocean. However, this period is of the order of 100 yr (Manabe and Bryan 1969), and the number of hours (nearly 150) of CDC 6600 computer time needed for such an experiment with our in-tandem model is impractically large. The use of seasonally variable solar heating casts doubt on the applicability of Manabe and Bryan's procedure of marching the ocean model forward many times faster than the atmosphere model, effectively computing with a much longer time scale in the ocean. We decided that the time scale of interest in our experiments was the 1-yr period of the heating cycle rather than the much longer thermal relaxation time of the ocean. For our purposes, then, adequate adjustment in the ocean would be signaled by the occurrence of low-latitude 1-yr surface temperature fluctuations at constant lag with respect to the solar forcing.

Two 3-yr experiments were made with the new, simple, and efficient interacting model; they differed only in the initial and boundary conditions. In the atmosphere, two sets of such conditions were established in which we used the atmospheric climatological data of Kidson et al. (1969). In one case, mean values of real Northern and Southern Hemisphere zonally averaged data were used in both model hemispheres and in the other case, each real hemisphere's data were used in the corresponding model hemisphere. The former case may be called initially symmetric while the latter case was initially asymmetric. Both sets of initial conditions represented annual means in the interior and on the boundaries. Both sets of lateral boundary conditions, at latitudes 30°N and 30°S, consisted of variables fluctuating sinusoidally about their annual means with a period of 1 yr and with amplitudes according to climatology. In the sea, both the symmetric and the asymmetric initial surface temperature profiles were obtained from Wyrtki's (1964) east-central Pacific data at longitude 140°W modified to eliminate the observed equatorial cool zone. In the 3-yr experiments, all the oceanic predictive equations were applied at the lateral boundaries, assuming zero gradients of the predicted properties poleward of these boundaries.

In the atmosphere model, the initial pressure field was obtained from the initial potential temperature field by prescribing in all cases an initially hemispherically symmetric surface pressure profile

$$p_s(x)=1015-5\cos\left(\frac{\pi x}{x_{30}}\right)\quad\text{(mb)} \tag{23}$$

and then integrating eq (6) upward. The initial wind field was computed from the resulting pressure field by assuming the wind to be zonal, geostrophic, horizontal, and nondivergent. On the Equator, the first x-derivative of the geostrophic wind equation was used to obtain an initially balanced wind that was proportional to the *second* x-derivative of pressure. Initial specific humidities were computed by assuming the initial relative humidity to be a function of height only and to be equal to the values given by Jordan (1958) for the annual mean tropical atmosphere. In the oceanic model, the initial mixed-layer depth and underlayer temperature profiles were given by eq (13) and (14) of Pike (1971); the initial current was obtained by using the same assumptions made for the initial atmospheric winds.

The following values of the various adjustable atmospheric constants were used in both 3-yr experiments;

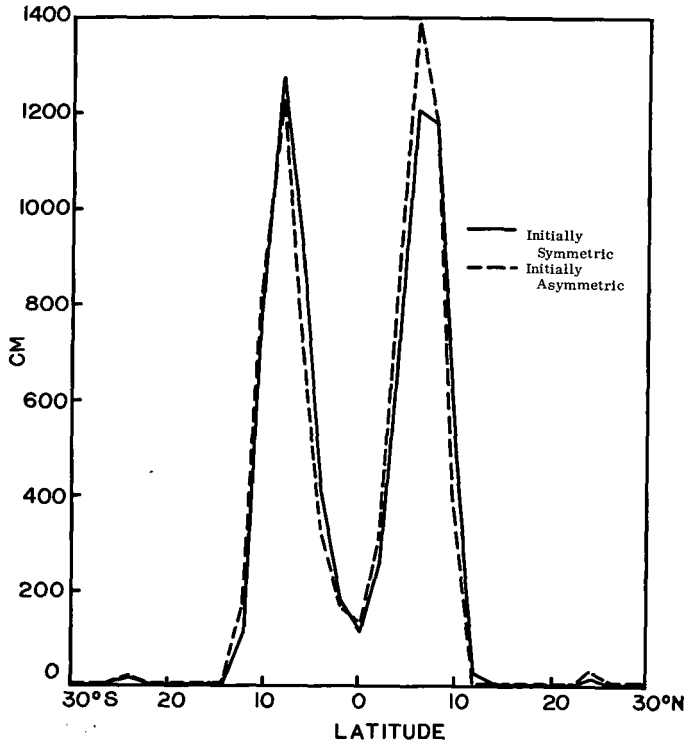

FIGURE 1.—The 3-yr accumulated precipitation profiles for long-term interacting experiments.

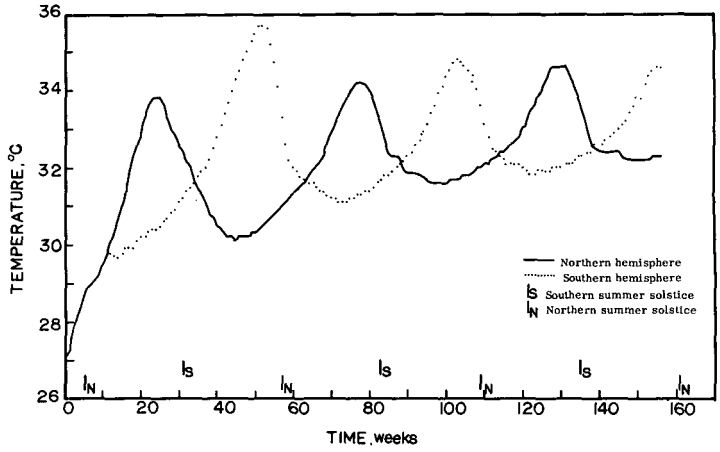

FIGURE 2.—Seasonal variation of maximum subequatorial surface temperature in both hemispheres for the initially symmetric experiment.

surface drag coefficient, $C_D=1.0\times10^{-3}$, vertical atmospheric diffusivity $K_z=2\times10^4$ cm^2/s, moisture condensation fraction $l=0.34$ [i.e., Yamasaki's (1968) value for our vertical grid levels in a mean tropical atmosphere], and horizontal atmospheric diffusivity $K_H=10^{10}$ cm^2/s (from Murgatroyd 1969). The radiational cooling $(\partial T/\partial t)_R$ in eq (12) was taken as -0.45°C/day at the 0.010-, 1.057-, and 5.870-km levels and zero elsewhere. This cooling rate in the atmosphere model interior was chosen so that the integrated atmospheric enthalpy [eq (24)] would be kept nearly constant over a 2-week test run, but it proved to be too slow in the longer term. The initial thermal lag time, t_p, was set at 8 weeks and t_v was assumed to be 52 weeks. In the ocean model, the horizontal mixing coefficient, k_0, was 0.80 as in our earlier work.

Very similar results were obtained from the initially symmetric case and the initially asymmetric case. Figure 1 shows the superimposed 3-yr accumulated precipitation profiles for both cases. We find little difference between them except for minor variations that may be ascribed mostly to numerical errors. Note the two well-defined precipitation peaks at latitudes 6°N and 8°S separated by a well-marked equatorial minimum. These two maxima and the minimum are intimately associated with, respectively, the warm subequatorial and the cold equatorial sea-surface temperatures that all our interacting model experiments predict.

Because of the basic similarity between the two 3-yr cases, further discussion will be limited to the initially symmetric experiment. It is apparent that hemispheric asymmetries in the real atmosphere are essentially three dimensional, with the different distributions of land and sea influencing the different atmospheric eddy characteristics of the two hemispheres that in turn influence the different zonal mean structures (Dickinson 1971). The relative simplicity of our model, restricted as it is to meridional plane dynamics with no zonal–meridional eddy correlations, suggests that its results be presented at least as much in their own right as in comparison with the real atmosphere.

The quasi-symmetrical rainfall profiles of figure 1 should *not* be interpreted as being produced by a double ITCZ of approximately equal strength in both hemispheres at any one time. Instead, the double precipitation peak has been caused by a single ITCZ that establishes itself over the surface temperature maximum in the warmer hemisphere and migrates quickly across the cool Equator into the opposite hemisphere whenever the progression of the seasons causes the hemispheric thermal asymmetry to reverse. Figure 2 shows the maximum surface temperature in the subequatorial warm zone (latitude 5°–10°) of each hemisphere as a function of time. Note that the seasonal variation becomes very clear and that the two hemispheres are nicely out of phase. The lag of each hemisphere's maximum subequatorial temperature behind the corresponding summer solstice is computed to be 20 weeks. The overhead sun of late summer occurs at these latitudes about 11 weeks after this solstice; therefore, the oceanic thermal lag behind the maximum solar heating of late summer is about 9 weeks, or 2 mo—a reasonable value. Apparently, the relatively small decrease of solar heating that follows the overhead sun of early spring is not sufficient to force a double maximum in the annual variation of the low-latitude sea-surface temperature. The ocean's large thermal lag tends to smooth the temperature versus time curve to show only one maximum each year, at least in our model.

Unfortunately, there are no accurate long-term observations of the progression of sea-surface temperature with time in very low latitudes to definitely confirm these particular lag characteristics. However, the data of Wyrtki (1964) for the eastern Pacific do suggest a hemispherically averaged surface thermal lag behind the second

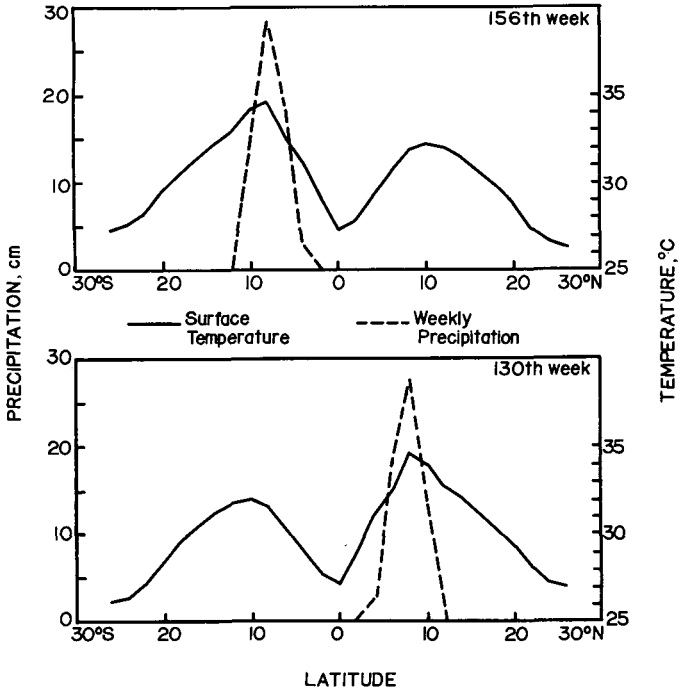

FIGURE 3.—Surface temperature and precipitation profiles for two cases 1/2 yr apart.

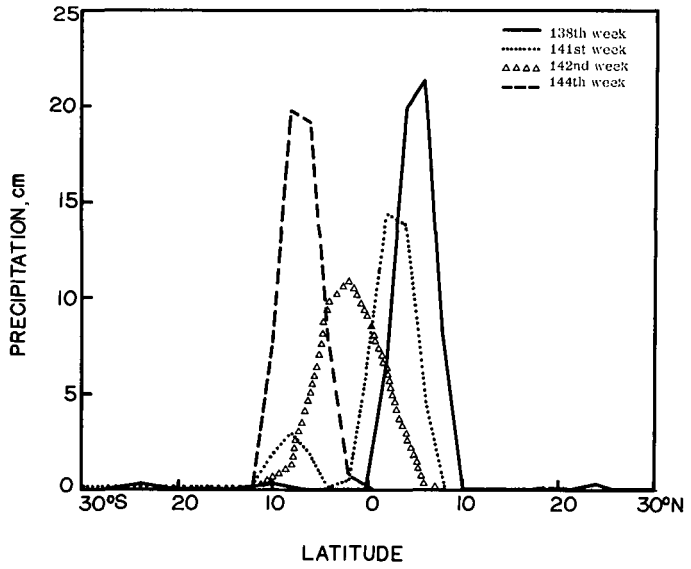

FIGURE 4.—Precipitation profiles illustrating ITCZ transition between hemispheres.

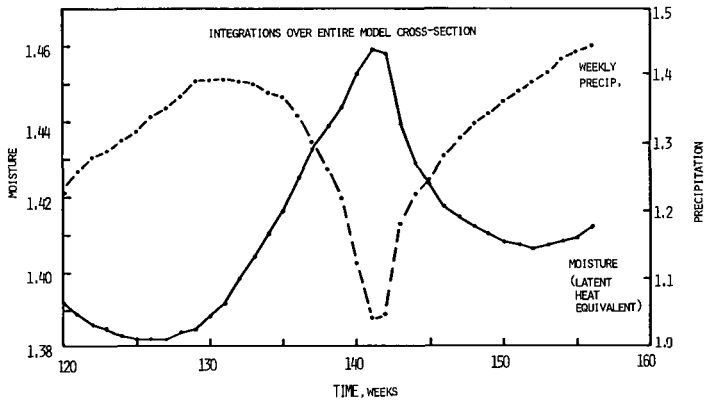

FIGURE 5.—Integrated precipitation (10^9 cm^2) and moisture (10^{13} J/cm) variations during ITCZ transition between hemispheres.

overhead sun of between 1 and 2 mo at these latitudes. The observed Southern Hemisphere lag seems to be larger than that in the Northern Hemisphere, in agreement with the lesser continental influence there. In both hemispheres, only one sea temperature maximum per year is observed, in agreement with the model results.

Note that the computed surface temperatures in this 3-yr experiment rise to about 5°C above the initial, climatological value. Some possible reasons for such excessive warming will be discussed later in this section.

The dependence of the location of our model's single ITCZ upon the nature of the surface temperature profile is graphically illustrated in figure 3. Recall from figure 2 that the Northern and Southern Hemisphere surface temperatures were last passing through maxima at respectively the 130th and 156th week, 1/2 yr apart. In figure 3, the temperature and precipitation profiles for these two periods are shown; in each case, the ITCZ is single and is located over the surface temperature maximum in the warmer hemisphere. These two cases are practically mirror images of each other. One may easily imagine how the quasi-symmetric rainfall profiles of figure 1 have been generated by the single ITCZ alternating between hemispheres according to which is warmer.

Whenever the hemispheric temperature asymmetry reverses, as at the 140th week (fig. 2), the model ITCZ shifts from one hemisphere to the other with only a minor lag. Figure 4 illustrates this process with four successive precipitation profiles. At the 138th week, the Northern Hemisphere is still definitely the warmer; its single ITCZ at latitude 6°N is well marked. A very weak convergence zone is indicated at latitude 10°S. Three weeks later, the Southern Hemisphere has become just a little warmer than the Northern Hemisphere; at this time, the ITCZ has taken on a transitory double structure with the old northern convergence zone approaching the Equator and weakening over the relatively cold water while a new, southern convergence zone is developing at latitude 8°S. By the 142d week, the ITCZ is again single, though still in a somewhat depressed state, and has clearly moved across the Equator into the warmer Southern Hemisphere. Two weeks later, equatorial rainfall has ended, and a single, reinvigorated ITCZ is well established at latitude 8°S.

The reduction in ITCZ precipitation during the period of transition between hemispheres is significant; the total rainfall rate, proportional to the scaled area beneath the precipitation curves of our figures, passes through a minimum at the 141st week that is fully 26 percent less than the mean rate of the 130th and 156th weeks (fig. 5). Recall that, during these 2 weeks, the hemispheric thermal asymmetry was most pronounced and the ITCZ was well developed. One physical reason for this temporary reduction is clear; during its transition across the Equator, the ITCZ passes over the cooler equatorial water and is ex-

posed to a reduced moisture source. This ITCZ weakening over the Equator may be related to the lack of boundary layer pumping there as supposed by Charney (1969). But, it is easy to visualize low-level convergence at the Equator, even under a uniform easterly flow aloft, as a result of the opposite directions of frictional turning in the two hemispheres. We note that Charney's simplified momentum equations are not strictly valid directly on the Equator and that our primitive-equation computations do not show anything like a complete collapse of the ITCZ when it moves over the Equator. Also recall that case I of section 2 of Pike (1971) showed an active, stable ITCZ directly over the Equator when there was no significant surface temperature depression there. Although the moist ITCZs of Bates (1970) did form away from the Equator with no such depression, his assumption of no available equatorial moisture [his eq (24)] excluded a *moist* ITCZ there a priori. Bates' *dry* ITCZ developed on the Equator. See Pike and Bates (1971) for more detail.

One would expect that, whenever the ITCZ is precipitating less, the total moisture stored in the tropical atmosphere might be increased because of the reduced condensation sink. To a relatively small extent, this situation does happen in our model. At 141 weeks when the ITCZ is weakest, the total moisture integrated over the whole model cross-section passes through a maximum that is 5 percent greater than the average of the minima achieved at 126 and 152 weeks. Because this maximum occurs 6 weeks after a solstice, at midwinter in one hemisphere and midsummer in the other, the increase in stored moisture just might supply extra available potential energy for extratropical storm development in the higher latitudes of the winter hemisphere and for tropical storm development in the subtropical latitudes of the summer hemisphere. Such three-dimensional phenomena cannot, of course, appear in these experiments.

However, nothing analogous to the "equinoctial storms" effect discussed and modeled by Kraus and Lorenz (1966) was noted in our calculations. As presented in their article, the regular, smooth, early autumnal increase in observed atmospheric zonal available potential energy was climaxed by the development of storminess. The broad wintertime peak in this potential energy was therefore very jagged; frequent baroclinic developments were intermittently reducing the stored energy. In our long-term experiments, however, the peak in stored atmospheric moisture coinciding with the temporary weakening of the ITCZ over cool equatorial waters was narrow but quite smooth with no apparent indication of jaggedness from brief bursts of ITCZ activity (fig. 5). Note also in this figure that ITCZ strength, as measured by the integrated precipitation, varied inversely with the stored moisture and in an equally smooth manner. The recovery of ITCZ activity after the ITCZ crossed the Equator was not significantly more rapid than was its earlier decline. A likely explanation for this smoothness is the rapidity with which the model ITCZ shifts between hemispheres; the stored moisture has an opportunity to increase only a few percent above its minimum value in contrast to the tripling of observed zonal available potential energy discussed by Kraus and Lorenz.

Probably the most disappointing aspect of the 3-yr experiments discussed above is the excessive warming of the sea surface and the resulting overheating of the atmosphere. Several shorter term computations with the simplified interacting model have been carried out in an attempt to remedy this problem. Because the oceanic heat balance in the upper layer of the model is composed primarily of incoming solar radiation and outgoing latent and sensible heat, we decided to modify the adjustable parts of the model involved with these processes.

The solar heating in our model is very sensitive to the computed cloudiness, a function of the vertically averaged relative humidity that in turn is partially dependent on the net radiative cooling. Because the arbitrary specification of the vertical radiative cooling profile used in the 3-yr experiments was not particularly satisfying, it was decided that the modeling of this persistent effect should play the role of a negative feedback, which ought to help stabilize the model thermally. It seemed reasonable to assume that, if $H_e(t)$ represents the total integrated enthalpy over the entire atmospheric cross-section of the model at time t according to

$$H_e(t)=\int_{x_{-30}}^{x_{30}}\int_0^H \rho c_p T(t)\,dz\,dx, \tag{24}$$

then $H_e(t)$ should be set equal to $H_e(0)$ at all times because the cross section is equally divided between hemispheres and one would expect its heat content to be very nearly conserved. If the radiational effect is given as a function of height by

$$\left(\frac{\partial T}{\partial t}\right)_R=\dot{T}_{R0}f(z), \tag{25}$$

then the integral in eq (24) may be conserved by letting

$$\dot{T}_{R0}=\frac{H_e(0)-H_e(t)}{\Delta t\int_{x_{-30}}^{x_{30}}\int_0^H \rho c_p f(z)\,dz\,dx}. \tag{26}$$

The vertical shape function, $f(z)$, has been specified as 0.0, 0.5, 0.8, 1.0, and 0.0 from the surface upward through the atmospheric model's vertical grid levels to the tropical tropopause. This profile is in agreement with the nature of the net radiative cooling as a function of height given for latitude 15° by Smagorinsky et al. (1965, p. 746). Equations (24)–(26) have been used in all our more recent model calculations with the maximum cooling $\dot{T}_{R0}$ being calculated at approximately −1.0°C/day, a reasonable amount.

Modification of the surface evaporative and sensible heat fluxes may clearly be achieved by changing the surface drag coefficient, C_D, in eq (8). These fluxes should be augmented by increasing C_D if surface cooling is the objective. Such an increase may also require a larger vertical turbulent diffusivity, K_z, to avoid trapping moisture in the surface boundary layer. The sea-surface temperature profiles of figure 6 illustrate how sensitive

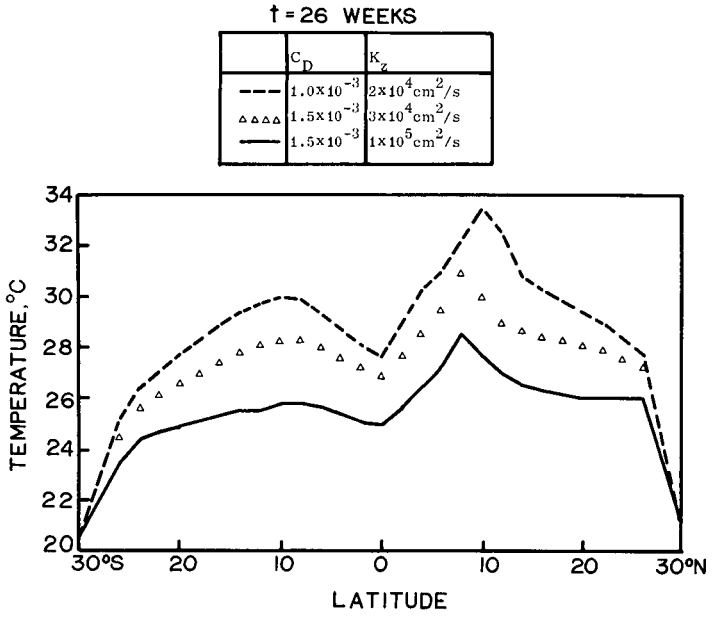

FIGURE 6.—Sea-surface temperature (°C) profiles illustrating the importance of vertical exchange coefficients.

this variable is to the adjustable coefficients of the vertical exchange processes. Three short-term experiments (each 26 weeks of model time), were made to produce these profiles. Although the case with $C_D=1.5\times10^{-3}$ and $K_z=10^5$ cm^2/s may seem the coolest and the most realistic, these relatively low temperatures were partly influenced by excessive moistening of the middle atmosphere and the resultant prediction of increased cloudiness and reduced surface solar insolation caused by the large vertical diffusivity. This case also exhibited surface air temperatures higher than those of the sea surface; sensible heat was being diffused downward too vigorously. More satisfactory is the case with the same drag coefficient as above but with $K_z=3\times10^4$ cm^2/s. In this instance, the only problem was with moisture saturation at the 1.057-km level.

That such an important variable as the sea-surface temperature should be quite sensitive to the exact values chosen for the adjustable coefficients C_D and K_z is somewhat annoying. One must recall, however, that in a fully interacting model such as ours, the surface heat fluxes play a primary role in determining this temperature and that the above coefficients influence these fluxes as described in the previous two paragraphs. Inspection of figure 6 clearly reveals, however, that only the prevailing temperature level is affected by these coefficients; the shape of the temperature profile appears to be nearly independent of them.

One might be concerned that the persistent warming trend shown in figure 2 would incorrectly influence the effect of one season on the next. Note in this same figure, however, that the lag characteristics of the surface temperature become constant after the first solar heating cycle. This lag stability indicates that the computed *seasonal* variations have real meaning.

The surface current components and mixed layer depth predicted by the oceanic portion of our long-term computations have not been illustrated in this section; their profiles are qualitatively similar to those obtained in the short-term interaction experiment discussed in section 4 of Pike (1971). Persistent deepening of the mixed layer continued to be present in the 3-yr experiment. In an effort to control this problem as well as to have more realistic sea temperatures at the model's edges, the lateral boundary conditions in the sea have been changed to specification, rather than prediction, of the ocean current components, temperature, and mixed layer depth at latitudes 30°S and 30°N. Fixing the mixed layer depth at these points should allow the lateral diffusion term in the oceanic mass-continuity equation [eq (4) of Pike 1971] to operate more effectively in preventing excessive deepening. Recent experiments are encouraging in this respect.

4. COMPARISON OF RESULTS WITH SATELLITE AND CONVENTIONAL OBSERVATIONS

There have been some problems in comparing the detailed behavior of the ITCZ precipitation in our long-term experiments with satellite observations of the seasonal variation of ITCZ cloudiness in the real atmosphere. Sadler's (1969) zonally averaged cloud data indicate that, during the Northern Hemisphere summer, a pronounced single-cloudiness maximum is located at latitude 6°N with no sign of any secondary maximum in the tropical Southern Hemisphere. This situation happens to be in good qualitative agreement with the prevailing ITCZ structure in the model. However, during the Southern Hemisphere summer, the expected cloudiness maximum at latitude 8°S is accompanied by a maximum in the Northern Hemisphere, slightly closer to the Equator. This winter hemisphere maximum is less distinct than the one in summer but, in combination with the Southern Hemisphere feature, still suggests a smeared double ITCZ of a type never present in the computations. Some conventional observations of the mean meridional circulation, to be discussed later, indicate that the winter tropical cloudiness of the Northern Hemisphere is probably associated, on the zonal average, with less upward air motion and, therefore, with less rainfall, than is its Southern Hemisphere summer companion.

Another interesting paper by Sadler (1970) uses satellite photography to study the transitional period when ITCZ cloudiness is increasing in one hemisphere and decreasing in the other. In that study, the observed changes in monthly mean cloudiness from one month to the next during this period are greatest at the off-equatorial latitudes where the ITCZ has been or will become well formed in an approximately steady state. Intermonthly mean cloudiness changes at the Equator seem to be relatively minor. Sadler reasons from these observations that the ITCZ declines in one hemisphere while re-forming in the other without any cross-equatorial migration. Our model, on the other hand, does indicate a migration, occurring over a period of about 1 mo (fig. 4). The apparent discrepancy between these results may be resolved by noting that our experimental ITCZ weakens markedly while it is crossing the Equator so that the magnitudes of

rainfall rate or cloudiness changes at the Equator are less than at subequatorial latitudes. Also note that during interhemispheric migration, changes in ITCZ properties would be monotonic sufficiently far from the Equator, while at and near the Equator these properties would pass through extrema making their net changes relatively small over a sufficient lapse of time. We suspect that Sadler's averaging period may be too long to observe this kind of migration. With the aid of daily satellite pictures, Johnson (1969) observed frequent ITCZ movement across the Equator in the Indian Ocean region.

It is much easier to compare the results of our long-term model computations with conventionally derived observations of the mean meridional circulation of the Tropics (e.g., Kidson et al. 1969, Oort and Rasmusson 1970) than with any satellite cloud data. Kidson's tables and diagrams clearly show that the upward branch of the direct tropical Hadley cell is centered at about latitude 10°N during the Northern Hemisphere summer and at about latitude 5°S during the Southern Hemisphere summer. At these latitudes during winter, the mean vertical motion is very small, equivalent to that near a Hadley cell center in fact. Kidson et al. does not present observations for the transition seasons, but the data of Oort and Rasmusson show a very smooth migration of the tropical mean updraft across the Equator during these periods. One notable difference between our experiments and the observed seasonal Hadley circulation is that in the former the width of the precipitation zone in each hemisphere is only about 10° of latitude while in the latter the updraft width is almost twice as great. This relative broadening is surely a result of the process of zonal averaging in the presence of the variation of land-sea distribution with longitude. In any event, our model does seem to approximate the seasonal behavior of the real tropical Hadley circulation fairly well with respect to location and structure. One would expect better results in this respect than those obtained when dealing with the actual three-dimensional ITCZ because of our two-dimensional dynamics.

The seasonal migration of this model's ITCZ is clearly related to the seasonal progress of its surface temperature. The same type of association is surely present in the real atmosphere. However, since the model's surface is purely oceanic while the earth's is partly continental, the lag characteristics (with respect to the solar heating) of the surface temperature and of the ITCZ will be different in the two cases. The real ITCZ rainfall is greatest over Africa, South Asia, and the adjacent islands (Dickinson 1971). Therefore, the lag behind the equinoxes of the migration of the mean tropical rain belt across the meteorological Equator is probably no more than 8 weeks, as confirmed by the vertical motion data of Oort and Rasmusson (1970). Over the real oceans, the lag of the local ITCZ is somewhat greater. For example, if one assumes that the oceanic ITCZ crosses the meteorological Equator at times halfway between the well-known Northern and Southern Hemispheric tropical storm activity peaks in September and March, respectively, the lag is about one season or 13 weeks. In our model, however, the tropical rainbelt is computed to cross the Equator, which in this case is meteorological as well as geographic, fully 20 weeks after each equinox (figs. 2 and 4). One should bear in mind that atmospheric circulations over the real oceans are not at all independent of those over the continents. Thus, even the oceanic ITCZ lag on earth should be expected to be less than that on a completely oceanic globe because of the relatively small surface-layer heat capacity on the continents. The 20-week lag seems to be physically realistic for our kind of model surface; it may be considered as the seven weeks' lag between the equinox and the maximum ocean temperature plus the mandatory one season's lag between the maximum and median ocean temperatures. Because the maximum model surface temperatures occur between latitudes 5° and 10° in space, they lag the overhead sun of late summer by about 2 mo in time.

It has been suggested that, since interhemispheric shifting of the real ITCZ is very seldom observed over the oceans except in the Indian Ocean region, such migration should not occur in a purely oceanic model like this one. The real oceans, however, are bounded by continents. The ITCZ's behavior over an unbounded ocean would probably not be similar to that over an ocean where fluid motions are subject to even subtle continental influences.

5. SUMMARY

Numerical integration of a combined atmosphere and ocean model over a period of several years seemed desirable for investigation of the degree of stability of the single off-equatorial ITCZ obtained in previous two-fluid experiments under the influence of seasonally variable solar heating of the sea. The atmospheric part of the original interacting model was simplified to such an extent that a 3-yr combined integration could be accomplished in about 4.5 hr of CDC 6600 computer time.

As before, a cold equatorial surface developed while a single ITCZ formed and soon found a stable location away from the Equator over the surface temperature maximum of the warmer hemisphere. The model ITCZ, in a temporarily weakened state, migrated quickly between hemispheres, with a lag of less than 2 weeks, whenever the progress of the seasons caused the hemispheric surface temperature asymmetry to reverse; that is, every half year. This behavior is qualitatively in accord with that of the updraft branch of the mean tropical Hadley circulation in the real atmosphere. The lag of the computed interhemispheric migration behind the solar equinox was 20 weeks, much longer than that of the observed mean tropical rainbelt, because of the lack of continents in our model. However, the lag of the maximum subequatorial sea-surface temperature behind the overhead sun of late summer was computed at 2 mo, a reasonable value for an ocean free of continental influences. These long-term experiments reinforced earlier results indicating that a single ITCZ is the preferred mode in our kind of model; this mode appears to be more common than any other in the real atmosphere as well.

ACKNOWLEDGMENTS

This research was sponsored under Contract No. F19628-68-C-0144 with the U.S. Air Force Cambridge Research Laboratories and Grant No. GA-26373 of the National Science Foundation.

Many thanks are due Eric Kraus, Mariano Estoque, Claes Rooth, and Stanley L. Rosenthal for many enlightening consultations. The IBM 360/65 computer at the University of Miami and the CDC 6600 at the National Center for Atmospheric Research, sponsored by the National Science Foundation, were used to make the numerical integrations. The manuscript of this paper was typed by Marcia Wilson and the figures were prepared by Lynn Gheer.

REFERENCES

Bates, J. Raphael, "Dynamics of Disturbances on the Intertropical Convergence Zone," *Quarterly Journal of the Royal Meteorological Society*, Vol. 96, No. 410, London, England, Oct. **1970**, pp. 677–701.

Budyko, Mikhail L., *The Heat Balance of the Earth's Surface (Teplovoĭ balans zemnoĭ poverkhnosti*, Akademii Nauk, Leningrad, U.S.S.R., 1956), N. A. Stepanova (Translator), U.S. Department of Commerce, Weather Bureau, Washington, D.C., **1958**, 259 pp.

Charney, Jule G., "The Intertropical Convergence Zone and the Hadley Circulation of the Atmosphere," *Proceedings of the WMO/IUGG Symposium on Numerical Weather Prediction, Tokyo, Japan, November 26–December 4, 1968*, Japan Meteorological Agency, Tokyo, Mar. **1969**, pp. III-73—III-79.

Dickinson, Robert E., "Analytic Models for Zonal Winds in the Tropics: II. Variation of the Tropospheric Mean Structure With Season and Differences Between Hemispheres," *Monthly Weather Review*, Vol. 99, No. 6, June **1971**, pp. 511–523.

Johnson, D. H., "The Role of the Tropics in the Global Circulation," *The Global Circulation of the Atmosphere*, Royal Meteorological Society, London, England, **1969**, pp. 113–136.

Jordan, Charles L., "Mean Soundings for the West Indies Area," *Journal of Meteorology*, Vol. 15, No. 1, Feb. **1958**, pp. 91–97.

Kidson, J. W., Vincent, D. G., and Newell, R. E., "Observational Studies of the General Circulation of the Tropics: Long Term Mean Values," *Quarterly Journal of the Royal Meteorological Society*, Vol. 95, No. 404, London, England, Apr. **1969**, pp. 258–287.

Kraus, Eric B., and Lorenz, Edward N., "Numerical Experiments With Large-Scale Seasonal Forcing," *Journal of the Atmospheric Sciences*, Vol. 23, No. 1, Jan. **1966**, pp. 3–12.

Manabe, Syukuro, and Bryan, Kirk, "Climate Calculation With a Combined Ocean-Atmosphere Model," *Journal of the Atmospheric Sciences*, Vol. 26, No. 4, July **1969**, pp. 786–789.

Murgatroyd, R. J., "Estimations From Geostrophic Trajectories of Horizontal Diffusivity in the Mid-Latitude Troposphere and Lower Stratosphere," *Quarterly Journal of the Royal Meteorological Society*, Vol. 95, No. 403, London, England, Jan. **1969**, pp. 40–62.

Oort, Abraham H., and Rasmusson, Eugene M., "On the Annual Variation of the Monthly Mean Meridional Circulation," *Monthly Weather Review*, Vol. 98, No. 6, June **1970**, pp. 423–442.

Pike, Arthur C., "Intertropical Convergence Zone Studied With an Interacting Atmosphere and Ocean Model," *Monthly Weather Review*, Vol. 99, No. 6, June **1971**, pp. 469–477.

Pike, Arthur C., and Bates, J. Raphael, "Correspondence—Comments on a Paper by J. R. Bates 'Dynamics of Disturbances on the Intertropical Convergence Zone,'" *Quarterly Journal of the Royal Meteorological Society*, Vol. 97, No. 413, London, England, July **1971**, pp. 350–351.

Richtmyer, Robert D., and Morton, K. W., *Difference Methods for Initial-Value Problems*, 2d Edition, Interscience Publishers, New York, N.Y., **1967**, 405 pp.

Sadler, James C., *Average Cloudiness in the Tropics From Satellite Observations*, East-West Center Press, Honolulu, Hawaii, **1969**, 23 pp.

Sadler, James C., "Does the Convergence Zone Migrate Between Hemispheres?" *Proceedings of the Symposium on Tropical Meteorology, Honolulu, Hawaii, June 2–11, 1970*, American Meteorological Society, Boston, Mass., **1970**, pp. F-IV-1—F-IV-7.

Smagorinsky, Joseph, "On the Dynamical Prediction of Large-Scale Condensation by Numerical Methods," *Geophysical Monograph* No. 5, American Geophysical Union, Washington, D.C., **1960**, pp. 71–78.

Smagorinsky, Joseph, Manabe, Syukuro, and Holloway, J. Leith, Jr., "Numerical Results From a Nine-Level General Circulation Model of the Atmosphere," *Monthly Weather Review*, Vol. 93, No. 12, Dec. **1965**, pp. 727–798.

Wyrtki, Klaus, "The Thermal Structure of the Eastern Pacific Ocean," *Deutsche Hydrographische Zeitschrift, Ergänzungsheft*, Ser. A, No. 6, Hamburg, Germany, **1964**, 84 pp.

Yamasaki, Masanori, "A Tropical Cyclone Model With Parameterized Vertical Partition of Released Latent Heat," *Journal of the Meteorological Society of Japan*, Vol. 46, No. 3, Tokyo, June **1968**, pp. 202-214.

[Received September 17, 1971; revised February 23, 1972]

467-299 O - 72 - 3